https://ntrs.nasa.gov/search.jsp?R=20100019446 2019-08-30T09:31:48+00:00Z

NASA/TM—2010-216369

Fatigue Resistance of the Grain Size Transition Zone in a Dual Microstructure Superalloy Disk

T.P. Gabb
Glenn Research Center, Cleveland, Ohio

P.T. Kantzos
Honeywell Engine Systems, Phoenix, Arizona

J. Telesman and J. Gayda
Glenn Research Center, Cleveland, Ohio

C.K. Sudbrack
Glenn Research Center, Cleveland, Ohio

B.S. Palsa
McGraw-Hill Companies, Inc., Columbus, Ohio

April 2010

NASA STI Program . . . in Profile

Since its founding, NASA has been dedicated to the advancement of aeronautics and space science. The NASA Scientific and Technical Information (STI) program plays a key part in helping NASA maintain this important role.

The NASA STI Program operates under the auspices of the Agency Chief Information Officer. It collects, organizes, provides for archiving, and disseminates NASA's STI. The NASA STI program provides access to the NASA Aeronautics and Space Database and its public interface, the NASA Technical Reports Server, thus providing one of the largest collections of aeronautical and space science STI in the world. Results are published in both non-NASA channels and by NASA in the NASA STI Report Series, which includes the following report types:

- TECHNICAL PUBLICATION. Reports of completed research or a major significant phase of research that present the results of NASA programs and include extensive data or theoretical analysis. Includes compilations of significant scientific and technical data and information deemed to be of continuing reference value. NASA counterpart of peer-reviewed formal professional papers but has less stringent limitations on manuscript length and extent of graphic presentations.

- TECHNICAL MEMORANDUM. Scientific and technical findings that are preliminary or of specialized interest, e.g., quick release reports, working papers, and bibliographies that contain minimal annotation. Does not contain extensive analysis.

- CONTRACTOR REPORT. Scientific and technical findings by NASA-sponsored contractors and grantees.

- CONFERENCE PUBLICATION. Collected papers from scientific and technical conferences, symposia, seminars, or other meetings sponsored or cosponsored by NASA.

- SPECIAL PUBLICATION. Scientific, technical, or historical information from NASA programs, projects, and missions, often concerned with subjects having substantial public interest.

- TECHNICAL TRANSLATION. English-language translations of foreign scientific and technical material pertinent to NASA's mission.

Specialized services also include creating custom thesauri, building customized databases, organizing and publishing research results.

For more information about the NASA STI program, see the following:

- Access the NASA STI program home page at *http://www.sti.nasa.gov*

- E-mail your question via the Internet to *help@sti.nasa.gov*

- Fax your question to the NASA STI Help Desk at 443–757–5803

- Telephone the NASA STI Help Desk at 443–757–5802

- Write to:
  NASA Center for AeroSpace Information (CASI)
  7115 Standard Drive
  Hanover, MD 21076–1320

NASA/TM—2010-216369

Fatigue Resistance of the Grain Size Transition Zone in a Dual Microstructure Superalloy Disk

T.P. Gabb
Glenn Research Center, Cleveland, Ohio

P.T. Kantzos
Honeywell Engine Systems, Phoenix, Arizona

J. Telesman and J. Gayda
Glenn Research Center, Cleveland, Ohio

C.K. Sudbrack
Glenn Research Center, Cleveland, Ohio

B.S. Palsa
McGraw-Hill Companies, Inc., Columbus, Ohio

National Aeronautics and
Space Administration

Glenn Research Center
Cleveland, Ohio 44135

April 2010

Acknowledgments

The authors wish to acknowledge the support of the NASA Aviation Safety Program. Disk forging was performed at PCC Wyman-Gordon Forgings under the direction of Ian Dempster. Disk heat treatments were performed at Ladish Forgings, Inc. under the direction of Joe Lemsky, and David Furrer, now at Rolls-Royce Aircraft Engines.

Trade names and trademarks are used in this report for identification only. Their usage does not constitute an official endorsement, either expressed or implied, by the National Aeronautics and Space Administration.

Level of Review: This material has been technically reviewed by technical management.

Available from

NASA Center for Aerospace Information
7115 Standard Drive
Hanover, MD 21076–1320

National Technical Information Service
5301 Shawnee Road
Alexandria, VA 22312

Available electronically at http://gltrs.grc.nasa.gov

Fatigue Resistance of the Grain Size Transition Zone in a Dual Microstructure Superalloy Disk

T.P. Gabb
National Aeronautics and Space Administration
Glenn Research Center
Cleveland, Ohio 44135

P.T. Kantzos
Honeywell Engine Systems
Phoenix, Arizona 85034

J. Telesman and J. Gayda
National Aeronautics and Space Administration
Glenn Research Center
Cleveland, Ohio 44135

C.K. Sudbrack
National Aeronautics and Space Administration
Glenn Research Center
Cleveland, Ohio 44135

B.S. Palsa
McGraw-Hill Companies, Inc.
Columbus, Ohio 43202

Abstract

Mechanical property requirements vary with location in nickel-based superalloy disks. To maximize the associated mechanical properties, heat treatment methods have been developed for producing tailored microstructures. In this study, a specialized heat treatment method was applied to produce varying grain microstructures from the bore to the rim portions of a powder metallurgy processed nickel-based superalloy disk. The bore of the contoured disk consisted of fine grains to maximize strength and fatigue resistance at lower temperatures. The rim microstructure of the disk consisted of coarse grains for maximum resistance to creep and dwell crack growth at high temperatures up to 704 °C. However, the fatigue resistance of the grain size transition zone was unclear, and needed to be evaluated. This zone was located as a band in the disk web between the bore and rim. Specimens were extracted parallel and transverse to the transition zone, and multiple fatigue tests were performed at 427 and 704 °C. Mean fatigue lives were lower at 427 °C than for 704 °C. Specimen failures often initiated at relatively large grains, which failed on crystallographic facets. Grain size distributions were characterized in the specimens, and related to the grains initiating failures as well as location within the transition zone. Fatigue life decreased with increasing maximum grain size. Correspondingly, mean fatigue resistance of the transition zone was slightly higher than that of the rim, but lower than that of the bore. The scatter in limited tests of replicates was comparable for all transition zone locations examined.

Introduction

In γ′ strengthened superalloys, solution heat treatments at temperatures sufficient to dissolve all existing γ′ precipitates allow enhanced grain growth (Ref. 1), as the precipitates no longer constrain grain boundaries. This behavior is especially evident in powder metallurgy disk superalloys (Ref. 2), where application of such a heat treatment after extrusion and forging can produce quite uniform grain sizes (Refs. 3 and 4). Disks heated to 20 to 40 °C below the γ′ solvus in "subsolvus" solution heat treatments retain 10 to 20 percent of coarse "primary" γ′ particles, which constrain grain growth to give uniform microstructures with grains near 5 to 10 μm in diameter. This fine grain size produces high strength and fatigue resistance at temperatures up to 550 °C, often typical requirements of disk bore and web regions. However, disks heated above the γ′ solvus in "supersolvus" solution heat treatments lose these constraining coarse "primary" γ′ particles, resulting in microstructures of larger grains near 30 to 70 μm in diameter. This coarse grain size gives lower strength and cyclic fatigue resistance, but improved time-dependent properties such as creep and dwell fatigue crack initiation and growth at application temperatures of 600 to 700 °C, typical requirements for disk rims in high performance turbine engines (Refs. 5 to 7).

The ability to vary the location specific microstructures to achieve a fine grain size in the bore and web of a disk, and coarse grain size in the rim of a disk, to maximize the associated mechanical properties as required at each location, is a promising approach to help optimize the disk design. Based on these perceived benefits, specialized heat treatment methods have been developed for producing tailored grain microstructures in the bore and rim portions of nickel-based superalloy disks (Refs. 5 to 7). The dual microstructure heat treatment (DMHT) method employed in the present study uses heat sinks to encourage a temporary temperature gradient between a disk's bore and rim regions, with the bore at lower temperature than the rim, Figure 1. When combined with finite element modeling and positioning of thermocouples at key locations, this allows design of solution heat treatments that limit the bore to subsolvus temperatures producing grain sizes of near 10 μm diameter (ASTM 11-12), while allowing the rim to reach supersolvus temperatures resulting in grain sizes of 30 to 80 μm diameter (ASTM 5-7). This allows disk grain microstructure to be varied in accordance with the property requirements of disk bore and rim locations. This process has been successfully demonstrated on four different advanced powder metallurgy disk superalloys (Refs. 7 to 10).

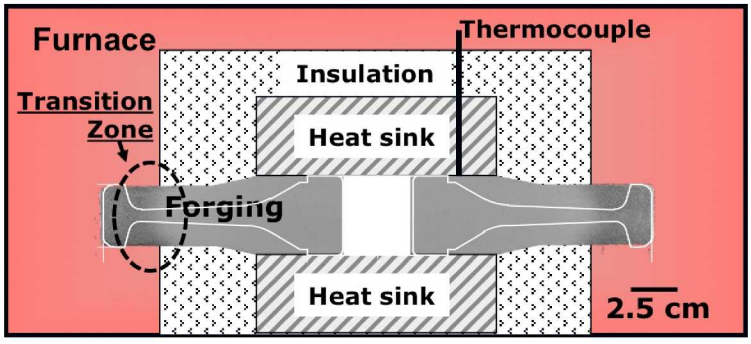

Figure 1.—Schematic of dual microstructure heat treatment (DMHT) assembly used for solution heat treatment of disk, with location of grain size transition zone indicated.

To validate the use of the DMHT process, it is necessary to verify the integrity of the transition zone by determining its fatigue resistance. The transition zone of the DMHT disk has a microstructure with variable grain size as a function of location. In coarse grain PM disk superalloys, fatigue failures can often initiate at grains which fail in a crystallographic manner due to concentrated slip (Refs. 11 and 12). These failing grains often appear to be relatively large with respect to the mean grain size for a given microstructure. Since grain size varies within the transition zone, it is important to determine the fatigue resistance and fatigue failure modes of the transition zone.

The objective of this study was to evaluate the low cycle fatigue resistance of the grain size transition zone in a DMHT disk. Specimens were extracted from the transition zone in the circumferential and radial directions. Grain size distributions were determined for each specimen location. Fatigue tests were performed at 427 and 704 °C to assess comparative fatigue lives and failure modes.

Materials and Procedure

Powder of low solvus, high refractory (LSHR) superalloy having the composition in weight percent of 3.5Al, 0.03B, 0.03C, 20.7Co, 12.5Cr, 2.7Mo, 1.5Nb, 1.6Ta, 3.5Ti, 4.3W, 0.05Zr, bal. Ni and trace impurities was atomized in argon by PCC Special Metals Corp. and passed through screens of –270 mesh to give powder particle diameters of no more than about 55 μm. The powder was then sealed in a stainless steel container, hot compacted, and extruded at a reduction ratio of 6:1 by PCC Wyman-Gordon Forgings. Segments of the extrusion billet were machined to segments approximately 15 cm diameter and 20 cm long, then isothermally forged into flat disks approximately 31 cm in diameter and 6 cm thick. A contoured disk was then machined with an outer diameter of 30 cm, maximum bore thickness of 5 cm, and rim thickness of 3.8 cm (Ref. 9). The disks were heat treated by Ladish Company, Inc. They were first conventionally subsolvus solution heat treated at 1135 °C for 2 h then air cooled, to give a uniform fine grain microstructure of ASTM 11-12. The DMHT process was then applied (Ref. 7), along with an aging heat treatment of 815 °C/8 h.

Specimen blanks were extracted as shown in Figure 2. Using rotational symmetry, they were located in three different tangential-oriented rings parallel to the transition zone of inner, mid, and outer radius, and in radial spokes perpendicular to the transition zone. Machining and testing of low cycle fatigue specimens, having a uniform gage diameter of 12.5 mm across a gage length of 19 mm, was performed by Mar-Test, Inc. and NASA GRC. The low cycle fatigue (LCF) specimens were tested using uniaxial closed-loop servo-hydraulic testing machines with induction heating and axial extensometers. Low cycle fatigue tests were performed at 427 and 704 °C.

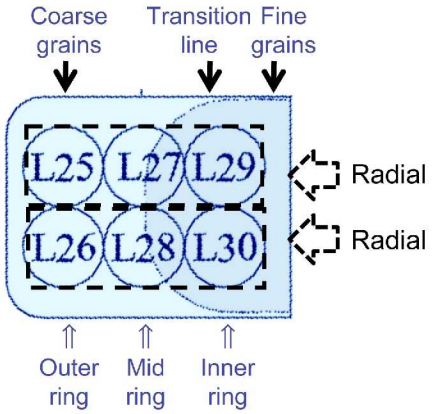

Figure 2.—Schematic showing location of inner, mid, and outer ring specimens in transition zone.

The maximum, minimum, and range of stresses generated during conventional strain-control fatigue tests can vary among repetition tests, due to slight differences in yield strength among individual specimens. Such variations in cyclic stress can influence fatigue life, and complicate comparisons of fatigue life between locations. Therefore, the first three fatigue tests for each specimen location were initiated with strain controlled to fixed limits. The remaining three tests were run with load controlled to fixed limits, to give a total of six tests performed for each location at each temperature. The first three of six tests for each location were performed according to ASTM E606, with strain initially controlled to fixed limits. A triangular waveform was employed for the first 6 h of cycling, varying strain at a frequency of 0.33 Hz over a total strain range of 0.6 percent at a strain ratio ($R_\varepsilon = \varepsilon_{min}/\varepsilon_{max}$) of 0. After 6 h of testing in this manner, surviving specimens were interrupted and then cycled using a triangular load-controlled waveform at a faster frequency of 10 Hz until failure, maintaining the stresses stabilized before interruption. The average stabilized maximum and minimum stresses were calculated for the three specimens tested in strain control for each specimen location and test temperature. These defined constant maximum and minimum stress limits for running the other three specimens of the group using a waveform controlling load, according to ASTM E466. A triangular waveform having a frequency of 10 Hz was employed here.

Fracture surfaces of all specimens were evaluated by scanning electron microscopy to determine crack initiation and propagation mechanisms. Grain sizes were determined on metallographically prepared sections. Linear intercept grain size distributions were determined from gage sections of representative test specimens according to ASTM E112 linear intercept procedures using circular grid overlays, grain area distributions were determined using image thresholding, and As-Large-As (ALA) grain sizes were determined according to ASTM E930. Grain size distributions and texture were also assessed using Electron Back Scatter Diffraction (EBSD), field emission scanning electron microscope equipped with a backscatter detector and EDAX (EDAX, Inc.) TSL electron backscatter diffraction analysis software.

Statistical analyses of variance were performed using JMP (SAS Institute, Inc.) software, with significance assessed at a probability $p = 0.05$, representing 95 percent confidence.

Results and Discussion

Material and Microstructures

Typical grain microstructures are shown in optical images from etched metallographic sections of LCF specimen sections, Figure 3. Linear intercept lengths for grains at each location are compared in Figure 4. Inner, mid, and outer ring specimens had increasing mean intercept grain diameters of 5.8, 38, and 55 μm, respectively, and had corresponding increasing ALA grain diameters of about 22, 410, and 413 μm, respectively.

The grain size transition zone was abrupt in this disk, and was usually captured within the gage cross sections of specimens at the mid location. Within this mid location, a bimodal grain size distribution mixing large and small grains was observed, giving a lower slope and more nonlinearity in cumulative probability versus log(grain size) than for inner and outer locations, Figure 4. The grain size—cumulative probability plots were comparable for individual specimens of a fixed location. Inner ring specimens also had coarse, undissolved "primary" γ′ particles widely spaced along grain boundaries and sometimes scattered within grains, Figure 3. As shown in Figure 3, the most abrupt plane of transition in grain size was located parallel to the loading axis in the gage sections of mid ring specimens. This shows as a line of transition in the image of a transverse section. However, this plane of grain transition was located normal to the loading axis near the middle of the gage sections in radial specimens. This shows as a line of transition in the presented image of a longitudinal section. This enabled fatigue loading of the grain size transition plane in the parallel and transverse directions, respectively.

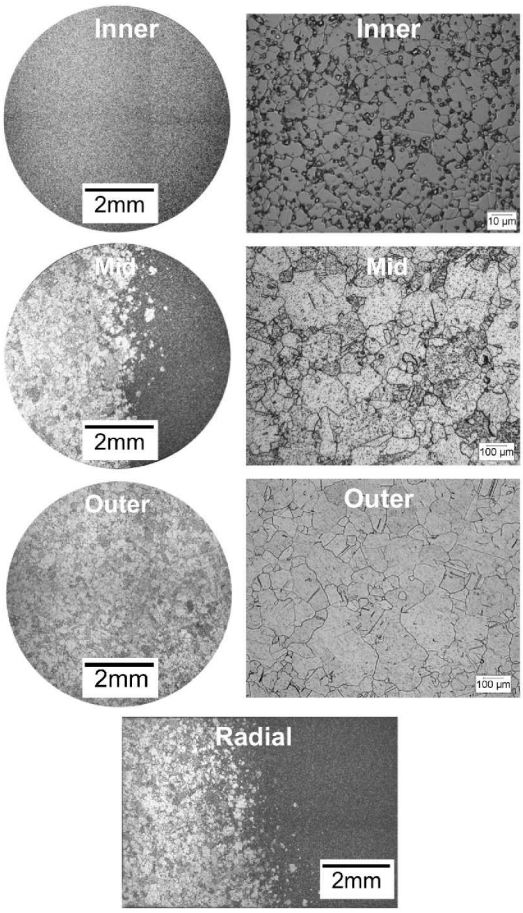

Figure 3.—Typical grain microstructures observed for inner, mid, and outer ring transition zone locations.

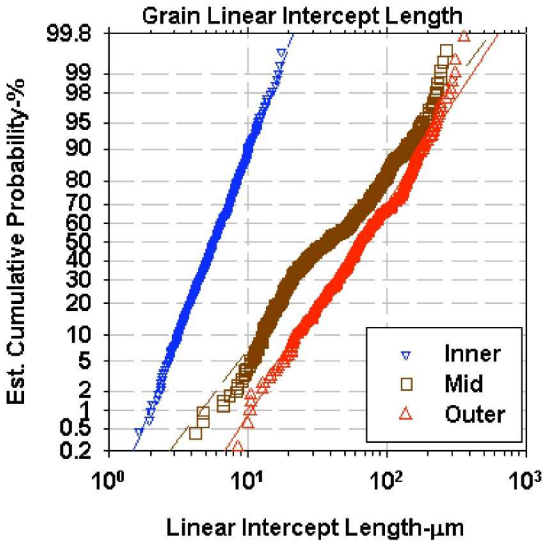

Figure 4.—Linear intercept grain size versus estimated cumulative probability of occurrence for inner, mid, and outer ring transition zone locations.

Low Cycle Fatigue Response

Fatigue life is compared for the different specimen locations within the transition zone in Tables 1 and 2, and in the cumulative probability plots of Figure 5. The fatigue lives have a log normal distribution as is evident by the linear fit of the data shown in a plot with a logarithmic life cycle axis. Modest scatter in life was observed for each specimen location. No difference was consistently observed between strain controlled (open symbols) and load controlled (filled symbols) test lives. The resulting lives were therefore grouped together in all analyses.

As shown in Figure 5, for tests conducted at both 427 and 704 °C, the inner location specimens had significantly higher mean fatigue lives than mid, outer, and radial specimens at both test temperatures. Inner specimens had over 10x higher mean lives than mid, outer, and radial specimens at 427 °C, and over 50x higher mean lives at 704 °C. Mid, radial, and then outer specimens ranked in order of decreasing mean fatigue lives at both test temperatures however the differences in lives between these three locations were relatively modest. Outer samples had lower mean lives than those of mid and radial specimens at the required 95 percent significance level for tests at 427 °C, but at lower significance levels in tests at 704 °C. One-way analysis of variance comparisons of log(life) comparisons showing the detailed statistical analysis of these observations is included in Appendix Table 1a.

TABLE 1.—FATIGUE TEST RESULTS AT 427 °C

Spec ID	Disk-Location	Temp-erature (C)	Starting Control Mode	Elastic Modulus (GPa)	Stress Range (MPa)	Max Stress (MPa)	Min Stress (MPa)	Smith-Watson-Topper Stress (MPa)	Fatigue Life (Cycles)	Prime Initiator Type	Prime Initiator Min. Depth (μm)	Prime Initiator Area (μm^2)	Prime Initiator Maj. Length (μm)	Prime Initiator Min. Length (μm)
L36	DMHT-Inner	427	Load		1165	1124	-41	809	290,379	Inclusion	2,650	639	36	29
L29	DMHT-Inner	427	Strain	198	1159	1132	-27	810	325,908	Inclusion	468	628	38	25
L5	DMHT-Inner	427	Strain	198	1173	1134	-39	816	327,202	Inclusion	1,636	711	43	23
L17	DMHT-Inner	427	Load		1165	1124	-41	809	349,760	Inclusion	48	176	24	10
L12	DMHT-Inner	427	Load		1165	1124	-41	809	355,313	Inclusion	352	67	19	5
L24	DMHT-Inner	427	Strain	197	1168	1116	-52	807	483,703	Facet	28	202	21	14
L33	DMHT-Mid	427	Strain	203	1204	1032	-173	788	24,505	Facet	173	28,579	355	122
L 4	DMHT-Mid	427	Load		1186	1055	-131	791	26,342	Facet	67	24,035	244	146
L28	DMHT-Mid	427	Load		1186	1055	-131	791	26,991	Facet	84	40,594	336	173
L21	DMHT-Mid	427	Load		1186	1055	-131	791	27,057	Facet	895	19,297	237	107
L9	DMHT-Mid	427	Strain	203	1189	1067	-123	796	27,061	Facet	262	30,386	297	172
L16	DMHT-Mid	427	Strain	201	1175	1082	-93	797	30,799	Facet	0	63,359	399	238
L 8	DMHT-Outer	427	Load		1172	993	-179	763	12,307	Facet	0	34,199	278	204
L20	DMHT-Outer	427	Strain	202	1180	1037	-142	782	14,881	Facet	0	72,257	372	287
L13	DMHT-Outer	427	Load		1172	993	-179	763	17,036	Facet	0	35,224	297	215
L37	DMHT-Outer	427	Strain	196	1160	1043	-117	778	18,463	Facet	0	18,518	182	164
L32	DMHT-Outer	427	Load		1172	993	-179	763	19,925	Facet	0	17,868	201	139
L1	DMHT-Outer	427	Strain	195	1161	951	-210	743	25,287	Facet	57	13,347	163	140
RL16	DMHT-Radial	427	Load		1186	1055	-131	791	18,898	Facet	91	69,345	438	311
R17	DMHT-Radial	427	Strain	205	1198	1074	-124	802	18,901	Facet	0	57,086	432	246
RL13	DMHT-Radial	427	Load		1186	1055	-131	791	22,010	Facet	96	16,887	208	160
RL 2	DMHT-Radial	427	Load		1186	1055	-131	791	22,921	Facet	151	27,332	254	170
R3	DMHT-Radial	427	Strain	201	1195	1041	-154	789	25,042	Facet	185	32,234	273	183
R6	DMHT-Radial	427	Strain	195	1163	1054	-108	783	31,883	Facet	352	15,180	315	70
A1 BL3	Supersolvus	427	Strain	206	1229	957	-272	767	48,725	Facet	0	7,547	111	94
A1 RL8	Supersolvus	427	Strain	196	1161	1014	-148	767	77,950	Facet	0	4,971	100	94
A1 BL4	Supersolvus	427	Strain	198	1182	880	-302	721	81,939	Facet	0	6,696	113	98
A1 BL5	Supersolvus	427	Strain	198	1166	933	-233	737	94,733	Facet	61	13,598	176	112

TABLE 2.—FATIGUE TEST RESULTS AT 704 °C

Spec ID	Disk-Location	Temp-erature (C)	Starting Control Mode	Elastic Modulus (GPa)	Stress Range (MPa)	Max Stress (MPa)	Min Stress (MPa)	Smith-Watson-Topper Stress (MPa)	Fatigue Life (Cycles)	Prime Initiator Type	Prime Initiator Min. Depth (μm)	Prime Initiator Area (μm^2)	Prime Initiator Maj. Length (μm)	Prime Initiator Min. Length (μm)
L6	DMHT-Inner	704	Strain	182	1074	1023	-51	741	1,062,332	Inclusion	1,333	973	59	23
L35	DMHT-Inner	704	Load		1062	1021	-41	736	1,072,677	Inclusion	2,283	451	38	25
L18	DMHT-Inner	704	Load		1062	1021	-41	736	1,130,332	Inclusion	951	598	43	23
L23	DMHT-Inner	704	Strain	178	1050	1025	-25	734	1,762,377	Inclusion	2,017	683	40	24
L30	DMHT-Inner	704	Strain	181	1067	1018	-49	737	1,834,651	Inclusion	1,983	1,346	61	36
L11	DMHT-Inner	704	Load		1062	1021	-41	736	2,635,233	Inclusion	398	489	38	20
L39	DMHT-Mid	704	Load		1055	986	-69	721	24,372	Smashed				
L 3	DMHT-Mid	704	Load		1055	986	-69	721	31,000	Facet	0	16,480	175	156
L22	DMHT-Mid	704	Load		1055	986	-69	721	34,519	Facet	36	55,352	343	241
L34	DMHT-Mid	704	Strain	181	1064	992	-72	726	35,736	Facet	69	13,350	174	131
L10	DMHT-Mid	704	Strain	179	1051	990	-61	721	63,939	Facet	589	36,701	326	184
L15	DMHT-Mid	704	Strain	178	1058	996	-63	726	94,741	Facet	146	23,169	210	177
L31	DMHT-Outer	704	Load		1055	966	-89	714	18,894	Facet	0	21,447	242	136
L19	DMHT-Outer	704	Strain	182	1076	993	-83	731	25,110	Facet	1,171	38,010	315	219
L14	DMHT-Outer	704	Load		1055	966	-89	714	26,125	Facet	80	25,131	219	174
L 7	DMHT-Outer	704	Load		1055	966	-89	714	29,635	Facet	1,485	51,533	379	251
L2	DMHT-Outer	704	Strain	181	1065	957	-108	714	31,168	Facet	1,137	42,561	345	179
L26	DMHT-Outer	704	Strain	175	1032	947	-85	699	37,300	Facet	352	7,105	127	79
RL14	DMHT-Radial	704	Load		1055	986	-69	721	21,998	Facet	0	33,147	310	204
RL 1	DMHT-Radial	704	Load		1055	986	-69	721	23,988	Facet	595	31,963	290	184
R4	DMHT-Radial	704	Strain	179	1055	969	-86	715	26,881	Facet	128	61,000	421	232
R5	DMHT-Radial	704	Strain	179	1051	981	-70	718	40,310	Facet	1,264	39,273	350	239
RL15	DMHT-Radial	704	Load		1055	986	-69	721	47,177	Facet	0	14,110	167	114
R18	DMHT-Radial	704	Strain	179	1058	991	-68	724	49,988	Facet	226	24,777	220	195
A1 BL7	Supersolvus	704	Strain	182	1077	925	-152	706	223,970	Facet	2,196	12,355	157	131
A1 RL7	Supersolvus	704	Strain	183	1091	980	-112	731	246,425	Facet	1,791	7,229	143	84
A1 BL6	Supersolvus	704	Strain	182	1088	985	-103	732	332,061	Facet	203	4,188	123	55

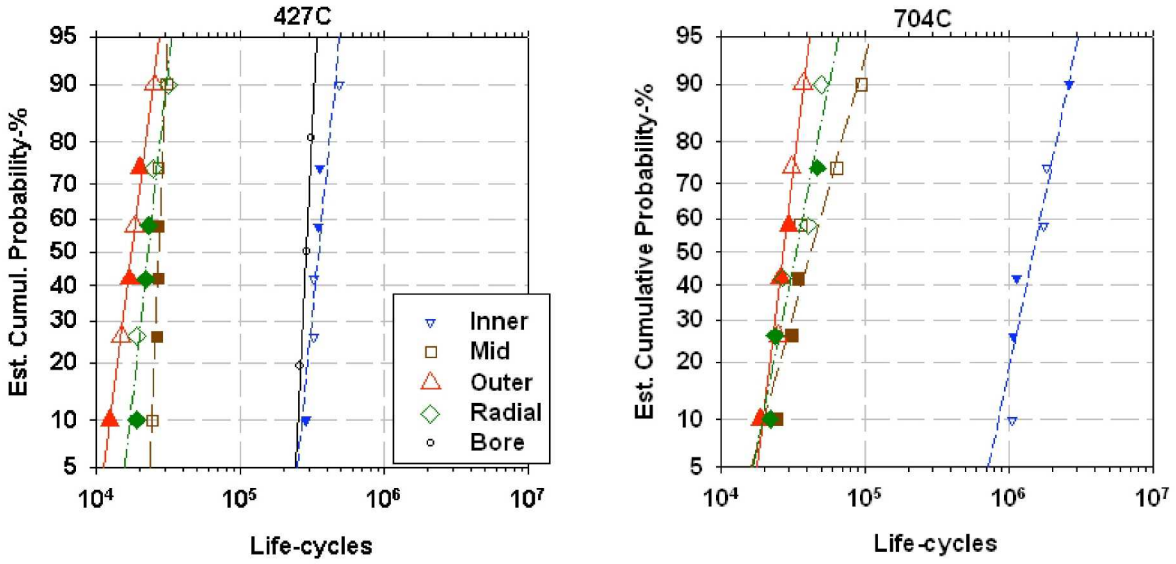

Figure 5.—Fatigue life versus estimated cumulative probability for tests at 427 and 704 °C. Strain-controlled tests are indicated in open symbols, fully load controlled tests by filled symbols.

Mean fatigue lives were significantly lower at 427 °C than at 704 °C for all transition zone specimen locations. This has been observed in other studies of this (Ref. 9) and other (Ref. 13) PM disk superalloys, and will be considered with respect to the failure modes and locations, and the stresses generated at each temperature. Several additional specimens extracted and tested from the bore of the disk had lives comparable to the inner ring specimens at 427 °C (Ref. 7); indicating fatigue life was likely stable over this inward region of the disk.

Failure Modes

Typical failure initiation sites are shown in Figure 6. Two predominant failure modes were observed. The fine grain inner ring specimens usually failed from small internal non-metallic inclusions. The inclusions initiating failures were usually granulated, aluminum-rich oxide Type 2 inclusions (Refs. 14 and 15). For the coarse grain outer specimens as well as mid and radial specimens which contained at least some coarse grain microstructure, the failures initiated at the crystallographic grain facets of large grains (Fig. 6(a)).

These crystallographic facet fatigue failures usually initiated near or at the specimen surface in tests of mid, outer, and radial specimens at 427 °C. However, several of these specimens failed from internal facet locations in tests at 704 °C, which resulted in longer lives than for surface initiated failures. This change of failure location with temperature can help explain the lower lives observed at 427 °C than for 704 °C. The facet failure mode, associated with the coarse grain microstructures, resulted in lower fatigue lives at both 427 and 704 °C than for inclusion- initiated failures of fine-grained inner and bore specimens.

Coarse grain microstructure is well known in these type alloys to decrease the low cycle fatigue life in comparison to fine grain microstructure. Here, not only did the coarse grain microstructure of the outer specimens result in low lives, but it also gave low fatigue lives for both the radial and mid specimens which contained both fine and coarse microstructures. For this apparent reason, radial specimens failed at locations corresponding to outer ring specimens, where larger grains were present to give earlier failures, Figure 7. Also, in case of the mid specimens, the crack initiation leading to failure was always located in the coarse grain section of the specimen cross section, also shown in Figure 7.

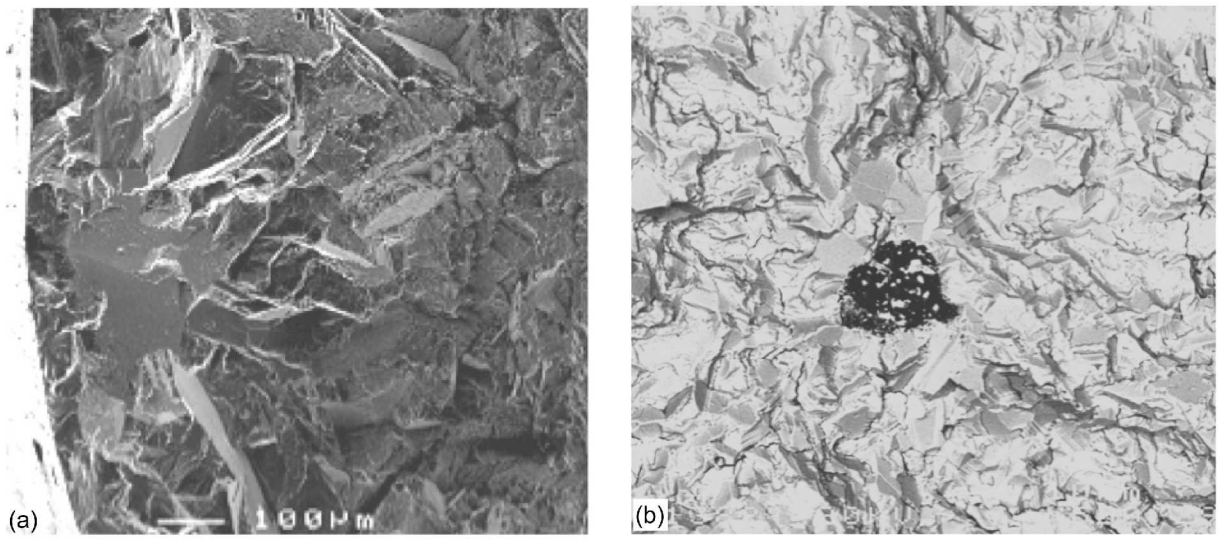

Figure 6.—Typical fatigue failure initiation sites: (a) grain facet failure initiating near the specimen surface of coarse grain specimens, (b) nonmetallic inclusion failure initiating away from the surface of fine grain specimens.

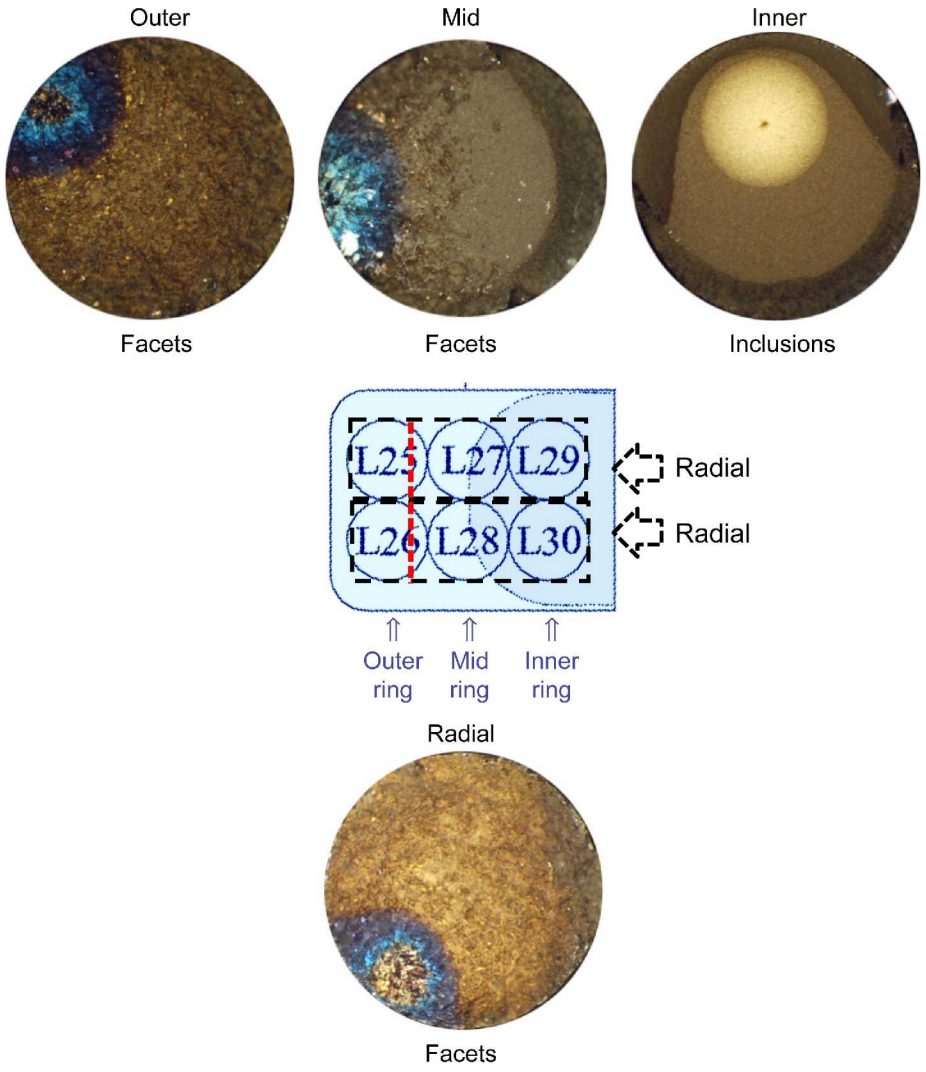

Figure 7.—Typical fatigue failure initiation sites: (a) facet failures initiating at coarse grains near or at the specimen surface for outer and mid specimens, internal inclusion failures for inner specimens, (b) near-surface facet failures at coarse grain ends (red lines) of radial specimens.

Fatigue Lives of DMHT and Uniform Grain Size Disks

In addition to the fatigue testing of the DMHT disk, fatigue tests were performed at these temperatures in a previous study of LSHR (Ref. 16), from disks of exactly the same chemistry, extrusion, and size, with microstructures having uniform grain. Comparisons of the results from these two studies can shed further light on the mechanisms governing low cycle fatigue behavior.

The uniform grain size disks had been given conventional isothermal subsolvus and supersolvus heat treatments, before the same 815 °C/8 h aging heat treatment used in the DMHT disk tested here. The observed fatigue lives from those isothermal subsolvus and supersolvus heat treated disks are compared to DMHT transition zone lives in plots of strain range versus life in Figure 8. DMHT inner ring and bore lives were comparable to that of the subsolvus disk. Yet, DMHT mid, outer, and radial specimens had consistently lower fatigue lives than those for the supersolvus disk.

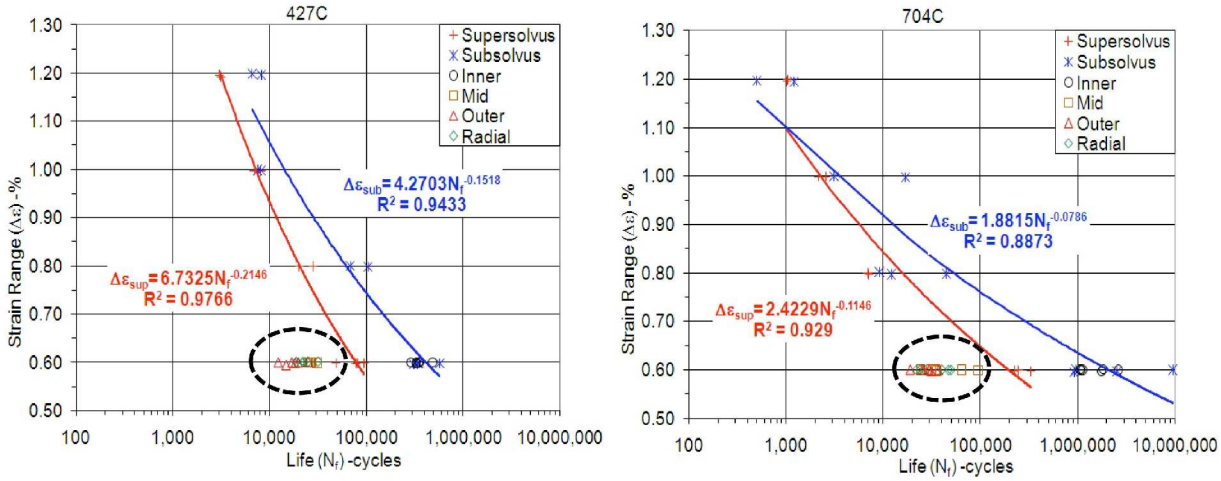

Figure 8.—Fatigue life versus total strain range for fatigue tests in transition zone of DMHT disk, compared to that for tests from uniform subsolvus fine grain and supersolvus coarse grain disks at 427 and 704 °C (Ref. 15).

Several issues were explored to gain an understanding why fatigue lives were lower for the DMHT disk at these transition zone locations than for the uniform supersolvus disk. Tensile and creep fatigue properties of the DMHT disk rim were previously determined to be comparable to those for the supersolvus disk (Ref. 9). The disks were also shown to have similar γ′ precipitate morphologies. However, the differences in fatigue life between the two disks could still be due in part to variations of cyclic stress range and mean stress response in fatigue tests of a given strain range. Such differences in cyclic stresses can be accounted for using a stress parameter proposed by Smith-Watson-Topper (Ref. 17):

$$SWT = (\sigma_{max}\Delta\sigma/2)^{0.5}$$

This relationship accounts for differences in maximum stress as well as stress range. Fatigue life is compared for these cases using SWT stress in Figure 9. No consistent variations in SWT stress versus life were observed that could account for the differences in life between the DMHT and supersolvus disks. However, SWT stresses were usually higher at 427 °C than for 704 °C at a given strain range, which could help explain the lower strain-life responses observed at 427 °C for both disks.

As previously described, the failures of the DMHT disk fatigue specimens were typically initiated on the crystallographic facets of large grains. The relationship between the size of the facets initiating failure and fatigue life for both the DMHT and supersolvus uniform grain size fatigue specimens was evaluated to ascertain the possible relationship between the facet size and fatigue life, Figure 10. As shown for both 427 and 704 °C, the fatigue specimens removed from the supersolvus disk had smaller facet sizes than those excised from the DMHT disk. Also note that the size of the facets seemed to be related to the corresponding fatigue lives, with the increase in size resulting in shorter lives.

One-way analysis of variance comparisons of log(facet area) indicated supersolvus specimens had significantly smaller mean facet areas than mid, outer, and radial specimens at both test temperatures, Appendix Table 2. The mean facet areas of mid, outer, and radial DMHT disk specimens did not differ significantly. This may explain the very small variation in mean fatigue lives for these three DMHT locations, as was noted earlier.

Facet sizes did not significantly vary between the two testing temperatures. Inner specimens had over 10x higher mean lives than mid, outer, and radial specimens at 427 °C, and over 50x higher mean lives at 704 °C. One-way analysis of variance comparisons of log(life) indicated supersolvus disk specimens correspondingly had significantly higher mean fatigue lives than mid, outer, and radial specimens at both test temperatures, Appendix Table 1. Increasing fatigue life significantly correlated with decreasing facet

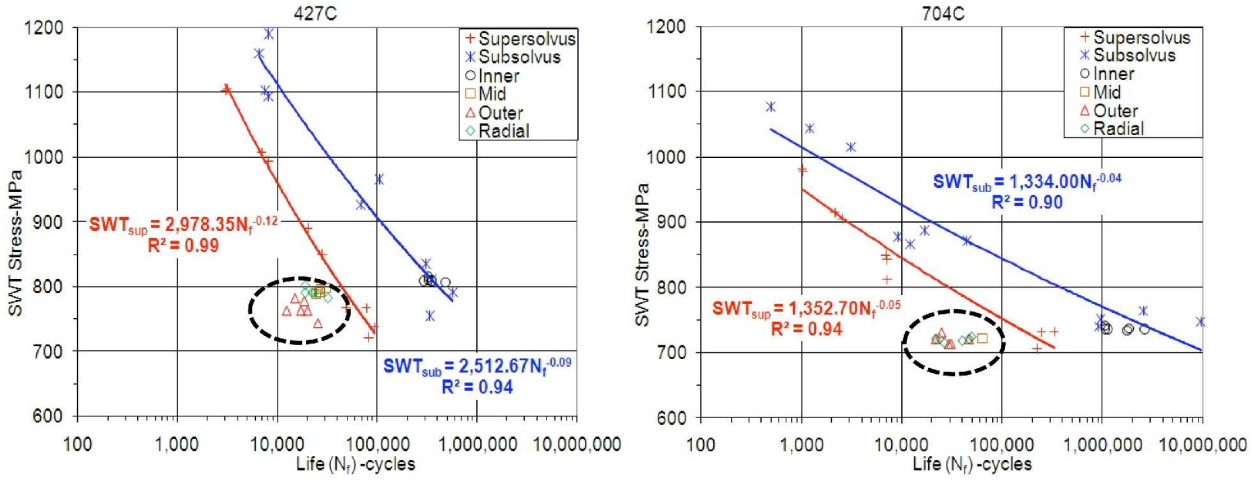

Figure 9.—Fatigue life versus Smith Watson Topper (SWT) stress for fatigue tests in transition zone of DMHT disk, compared to that for tests from uniform subsolvus fine grain and supersolvus coarse grain disks at 427 and 704 °C (Ref. 15).

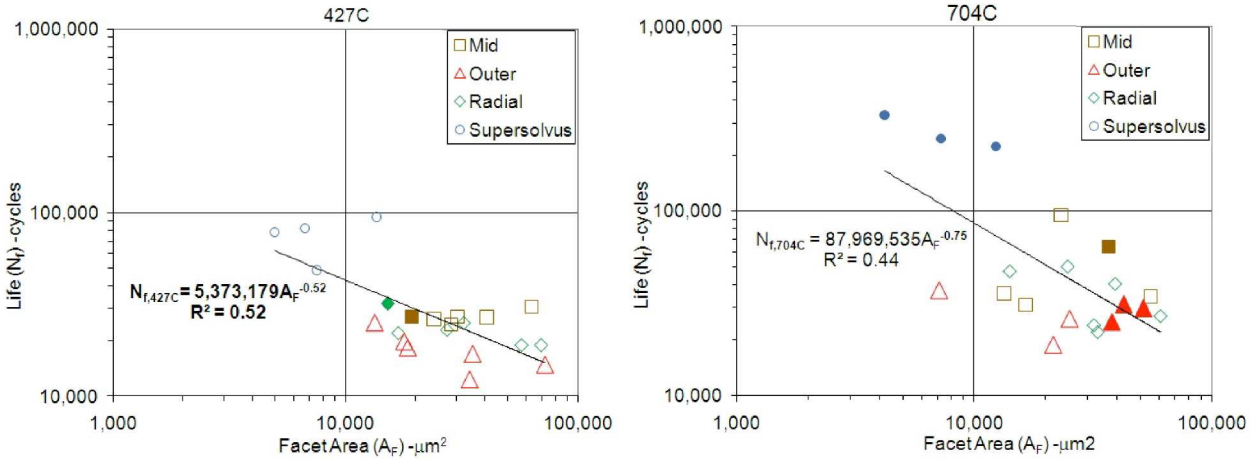

Figure 10.—Relationship of grain facet failure size versus life for DMHT and supersolvus disks at 427 and 704 °C. Open symbols indicate surface-initiated failures, filled symbols indicate internal-initiated failures.

size for all facet failures at both test temperatures. The correlation as indicated by the coefficient of determination was higher at 427 °C than for 704 °C. This appeared related in part to the locations of failure initiations. Most failure initiations were consistently near or at the surface for tests at 427 °C. However, several specimens failed from internal grain facets at 704 °C, producing lives significantly longer than surface failures. Such variations in life based on failure location have been observed in other disk superalloys (Refs. 13, 18, and 19).

The grain facet size was of course related to the grain size distribution of the samples. A micrograph of the grain structure in the supersolvus disk rim is shown in Figure 11. The mean linear intercept grain size of the supersolvus disk was approximately 33 µm, with an ALA grain size of 150 µm. Grain area size distributions are compared for DMHT mid and outer locations and the supersolvus disk in Figure 12. The grain area sizes of the supersolvus disk were significantly smaller than that of mid and outer ring specimens of the DMHT disk, due to the different heat treatment temperature-time paths of these two disks. Facet grain area sizes of the failed specimens are also included for mid, outer, radial, and supersolvus disk specimens in Figure 12. Grains causing facet failures were in the upper 30 percent of grain areas measured for each location. Thus, it was apparent that relatively large grains failed in

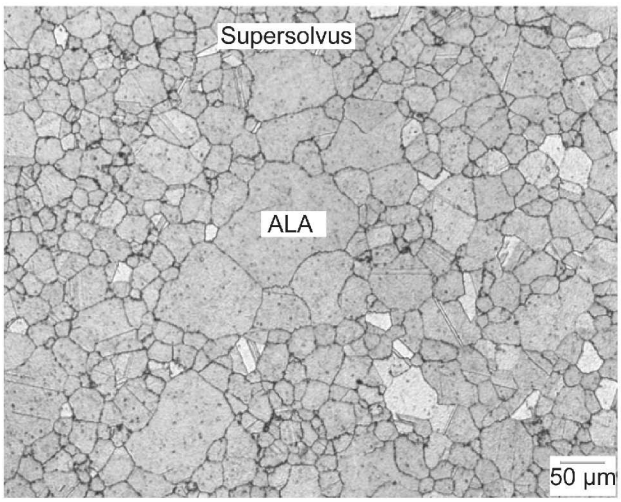

Figure 11.—Grain structure of supersolvus disk, showing ALA grain.

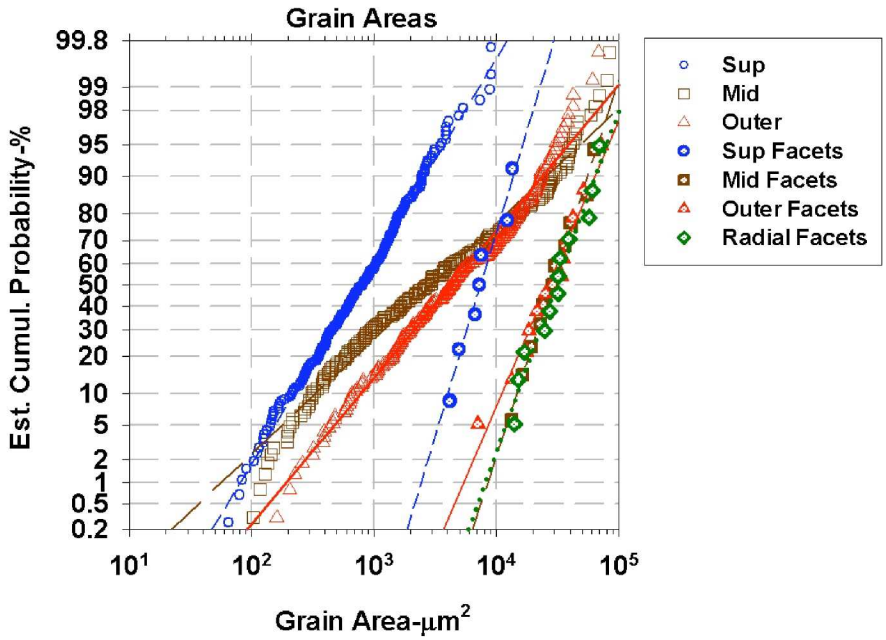

Figure 12.—Comparisons of overall and facet failure grain areas versus cumulative probability for mid, outer, and radial specimens tested at 427 and 704 °C.

specimens of each location. Such response has been observed in other disk superalloys (Refs. 11 and 12). It would be expected that crystallographic orientation of the large grains would also be important, to produce high resolved shear stress to cause facet failures on operative slip planes, and this was proven the case for high cycle fatigue failures of René 88DT in Reference 12. The stress state within a grain could also be affected by the resolved shear stresses of surrounding grains, including their magnitudes and orientations. But clearly, the relative large size of a grain was a first order determinant for facet failures in the current test conditions. Therefore, a properly calibrated correlation of facet size versus fatigue life at relevant conditions could perhaps be analytically combined with the measured distribution of grain sizes at a particular disk location, to generate a probabilistic life prediction.

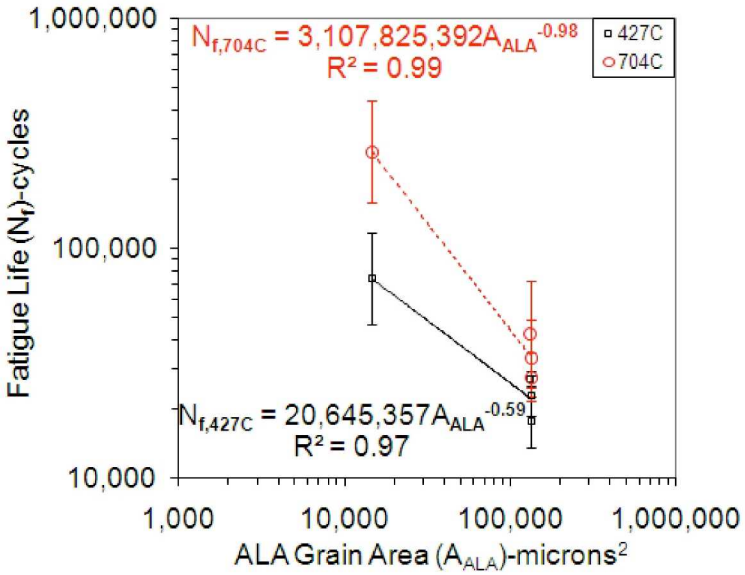

Figure 13.—Relationships of ALA grain area versus mean life for DMHT and supersolvus disk specimens tested at 427 and 704 °C.

It should be noted that grain texture and the percentage of twins and low angle grain boundaries were also compared for the supersolvus and DMHT disks. Texture, twin, and low angle grain boundary content were comparable for the supersolvus and DMHT mid and outer disk locations. Therefore, differences in grain size seemed to be mainly responsible for the differences in fatigue life between the DMHT transition zone and supersolvus disk specimens.

Since relatively large grains within the grain size distribution caused failures, ALA grain size (determined according to ASTM E930) could be used as a simple, well established measurement for bounding fatigue life in these conditions (Ref. 19). The correlation of mean fatigue life is shown versus ALA grain areas for the supersolvus disk and DMHT disks in Figure 13. ALA grain size correlated well with fatigue life at each temperature, and could be used as a practical predictor for upper bounds of facet grain size. However, it should be understood that facet size will approach, but often be smaller than actual ALA size, for each disk and specimen location.

Cyclic crack growth rates have been found to moderately decrease with increasing grain size in tests of this LSHR material, and decrease with decreasing temperature (Ref. 16). Therefore, the lower fatigue life of the coarser grain DMHT material could not be attributed to reduced crack propagation life, and must be linked in some way to reduced crack initiation life. The lower fatigue life observed at 427 °C compared to 704 °C has also been previously observed in this and other PM superalloys (Refs. 13 and 16), and also appears related to crack initiation life differences, including the greater propensity for surface facet failures and higher cyclic stresses observed at 427 °C. Interrupted testing would be necessary to fully confirm and understand how crack initiation life is reduced with increasing grain size and decreasing temperature in these materials.

Future Work

Additional work needs to be performed to improve the understanding and balance of microstructure-fatigue life relationships in the transition zone of disks having location-specific-microstructures, such as the DMHT disk process. Interrupted testing would allow better understanding of how crack initiation life is reduced with increasing grain size in these materials. Longitudinal sectioning could perhaps uncover multiple cracked grains, to allow an understanding of grain size, crystallographic orientation, and surrounding grain constraints necessary for fatigue crack initiation.

Such knowledge could then be applied to help guide enhancement of transition zone and rim microstructures and fatigue properties. Varied disk forging conditions have been found to significantly influence grain size response in powder metallurgy disk superalloys during subsequent heat treatments (Refs. 20 and 21). Therefore, varied forging conditions could be used to tailor grain size and fatigue properties in the transition zone and rim. Cooling rate and aging heat treatments have been found to strongly influence the balance of mechanical properties in most disk superalloys (Refs. 1, 2, 22, and 23), by altering the sizes and volume fractions of secondary and tertiary γ' precipitates. Modified heat treatments such as location-specific air quenching (Ref. 8) and increased aging time and temperature (Ref. 24) could be applied to potentially improve fatigue life of the transition zone.

However, cyclic fatigue crack initiation properties would need to be balanced with many other mechanical properties of importance for mechanical design of location specific microstructure disks. Depending on the location and service conditions of a transition zone, these could include cyclic fatigue crack growth, dwell fatigue crack initiation, dwell fatigue crack growth, and also strength and creep resistance, at both uniform and notched locations. Variations in grain microstructure at a fixed location of a location-specific-microstructure disk have been shown in the present study to have a key influence on cyclic fatigue life. Yet, some other mechanical properties such as tensile and creep resistance may be less sensitive to grain size variations.

Summary and Conclusions

The fatigue life, failure modes and microstructure of the transition zone of a DMHT disk were characterized using LCF testing, quantitative fractography, and metallography. Specimens located at an inner ring just within the transition zone had fatigue lives comparable to bore specimens, and were much longer than specimens located at mid and outer rings of the transition zone. The bore and inner ring specimens had a fine grain size and failed mostly from internal inclusions. The mid and radius specimens contained both coarse and fine grain size microstructures, but always failed from coarse grain facets. The coarse grain outer ring specimens also failed from large grain crystallographic facets. The grain facet failure initiations resulted in substantially lower fatigue lives.

The grain facets initiating failure were generally larger than the mean grain size, extending to near ALA grain size. The lives of specimens located mid way in the transition zone, with near bimodal grain size, appeared to still be limited by these large grains, with no additional complications due to wider grain size variations.

It can be concluded from this work that the cyclic fatigue failure response of the transition zone region behaves in a predictable manner for this DMHT disk, varying with maximum grain size for the current material and test conditions. Simple screening of mean and ALA grain size may be useful to initially estimate mean cyclic fatigue life in such location specific microstructure disks. Subsequently, a carefully calibrated correlation of facet size versus fatigue life could be analytically combined with measured distributions of grain sizes versus disk location, to then generate probabilistic life predictions. Thus, careful control, measurement, and then prediction of grain size distribution as a function of location will be important for accurate cyclic fatigue life prediction of DMHT and other disks having location-specific microstructures and mechanical properties. Several processing avenues may offer further refinements of microstructure for enhancing fatigue life. However, other mechanical properties need to be considered for such refinements and optimizations.

References

1. C.T. Sims, N.S. Stoloff, W.C. Hagel, Superalloys II, John Wiley & Sons, New York, NY, 1987, p. 477.
2. R.C. Reed, The Superalloys, Cambridge University Press, Cambridge, U.K., 2006, p. 242.
3. T.E. Volin, J.S. Benjamin, J.M. Larson, R.L. Cairns, "Thermoplastic Prealloyed Powder," U.S. Patent 3,930,841, U.S. Patent and Trademark Office, Washington, D.C., January, 1976.

4. J.L. Bartos, P.S. Mathur, "Development of Hot Isostatically Pressed (As-HIP) Powder Metallurgy René 95 Turbine Hardware," Superalloys: Metallurgy and Manufacture, ed. B.H. Kear, D.R. Muzyka, J.K. Tien, S.T. Wlodek, Claitor's Publishing Div., Baton Rouge, LA, 1976, pp. 495–508.
5. G.F. Mathey, "Method of Making Superalloy Turbine Disks Having Graded Coarse and Fine Grains," U.S. Patent 5,312,497, May, 1994.
6. S. Ganesh, R.G. Tolbert, "Differentially Heat Treated Article, and Apparatus and Process for the Manufacture Thereof," U.S. Patent 5,527,020, June, 1996.
7. J. Gayda, T.P. Gabb, P.T. Kantzos, "Heat Treatment Devices and Method of Operation Thereof to Produce Dual Microstructure Superalloy Disks," U.S. Patent 6,660,110 B1, U. S. Patent and Trademark Office, Washington, D.C., Dec., 2003.
8. J. Gayda, D.U. Furrer, "Dual Microstructure Heat Treatment," Advanced Materials & Processes, July, 2003, pp. 36–39.
9. J. Gayda, T.P. Gabb, P.T. Kantzos, "The Effect of Dual Microstructure Heat Treatment on an Advanced Nickel Base Disk Alloy," Superalloys 2004, ed. K.A. Green, T.M. Pollock, H. Harada, T.E. Howson, R.C. Reed, J.J. Schirra, S. Walston, The Minerals, Metals & Materials Society, Warrendale, PA, 2004, pp. 323–329.
10. R.J. Mitchell, J.A. Lemsky, R. Ramanathan, H.Y. Li, K.M. Perkins, L.D. Connor, "Process Development & Microstructure & Mechanical Property Evaluation of a Dual Microstructure Heat Treated Advanced Nickel Disc Alloy," Superalloys 2008, ed. R.C. Reed, K.A. Green, P. Caron, T.P. Gabb, M.G. Fahrmann, E.S. Huron, S.A. Woodard, TMS, Warrendale, PA, 2008, pp. 347–356.
11. T.P. Gabb, J. Gayda, J. Sweeney, "The Effect of Boron on the Low Cycle Fatigue Behavior of Disk Alloy KM4," NASA/TM—2000-210458, NASA, Washington, D.C., 2000.
12. J. Miao, T.M. Pollock, J. Wayne Jones, "Crystallographic Fatigue Crack Initiation in Nickel-based Superalloy René 88DT at Elevated Temperature," Acta Materialia, V. 57, 2009, pp. 5964–5974.
13. T.P. Gabb, J. Telesman, P.T. Kantzos, A. Garg, "Effects of Temperature on Failure Modes for a Nickel-Base Disk Superalloy," J. Failure Analysis and Prevention, V. 7, Feb. 2007, pp. 56–65.
14. D.R. Chang, D.D. Krueger, R.A. Sprague, "Superalloy Powder Processing, Properties, and Turbine Disk Applications," Superalloys 1984, ed. M. Gell, C.S. Kortovich, R.H. Bricknell, W.B. Kent, J.F. Radavich, The Minerals, Metals & Materials Society, Warrendale, PA, 1984, pp. 245–252.
15. R.L. Barrie, T.P. Gabb, J. Telesman, P.T. Kantzos, A. Prescenzi, T. Biles, P.J. Bonacuse, "Effectiveness of Shot Peening in Suppressing Fatigue Cracking at Non-Metallic Inclusions in Udimet 720," NASA/TM—2005-213577, Washington, D.C., March, 2005.
16. T.P. Gabb, J. Gayda, J. Telesman, P.T. Kantzos, "Thermal and Mechanical Property Characterization of the Advanced Disk Alloy LSHR," NASA/TM—2005-213645, Washington, D.C., June, 2005.
17. K.N. Smith, P. Watson, T.H. Topper, "A Stress-Strain Function for the Fatigue of Metals," Journal of Metals, V. 5, No. 4, 1970, pp. 767–778.
18. T.P. Gabb, J. Telesman, P.T. Kantzos, J.W. Smith, "Effects of High Temperature Exposures on Fatigue Life of Disk Superalloys," Superalloys 2004, ed. K.A. Green, H. Harada, T.E. Howson, T.M. Pollock, R.C. Reed, J.J. Schirra, S. Walston, TMS, Warrendale, PA, 2004, pp. 269–274.
19. M.L. Brogdon, A.H, Rosenberger, "Evaluation of the Influence of Grain Structure on the Fatigue Variability of Waspaloy," Superalloys 2008, ed. R.C. Reed, K.A. Green, P. Caron, T.P. Gabb, M.G. Fahrmann, E.S. Huron, S.A. Woodard, TMS, Warrendale, PA, 2008, pp. 583–588.
20. E. Huron, S. Srivatsa, E. Raymond, "Control of Grain Size Via Forging Strain Rate Limits for R'88DT," Superalloys 2000, ed. T.M. Pollock, R.D. Kissinger, R.R. Bowman, K.A. Green, M. McLean, S. Olson, J.J. Schirra, TMS, Warrendale, PA, 2000, pp. 49–58.
21. T.P. Gabb, J. Gayda, J. Falsey, "Forging of Advanced Disk Alloy LSHR," NASA/TM—2005-213649, Washington, D.C., June, 2005.

22. T.P. Gabb, J. Gayda, J. Telesman, A. Garg, "The Effects of Heat Treatment and Microstructure Variations on Disk Superalloy Properties at High Temperature," Superalloys 2008, ed. R.C. Reed, K.A. Green, P. Caron, T.P. Gabb, M.G. Fahrmann, E.S. Huron, S.A. Woodard, TMS, Warrendale, PA, 2008, pp. 121–130.
23. J. Telesman, T.P. Gabb, A. Garg, P. Bonacuse, J. Gayda, "Effect of Microstructure on Time Dependent Fatigue Crack Growth Behavior in a P/M Turbine Disk Alloy," Superalloys 2008, ed. R.C. Reed, K.A. Green, P. Caron, T.P. Gabb, M.G. Fahrmann, E.S. Huron, S.A. Woodard, TMS, Warrendale, PA, 2008, pp. 807–816.
24. J.R. Groh, "Local Heat Treatment for Improved Fatigue Resistance in Turbine Components," U.S. Patent Application 20,070,169,860, July, 2007.

Appendix—Analyses of Variance

TABLE 1a.—ONE-WAY ANALYSIS OF VARIANCE
FOR FATIGUE LIFE AT 427 °C

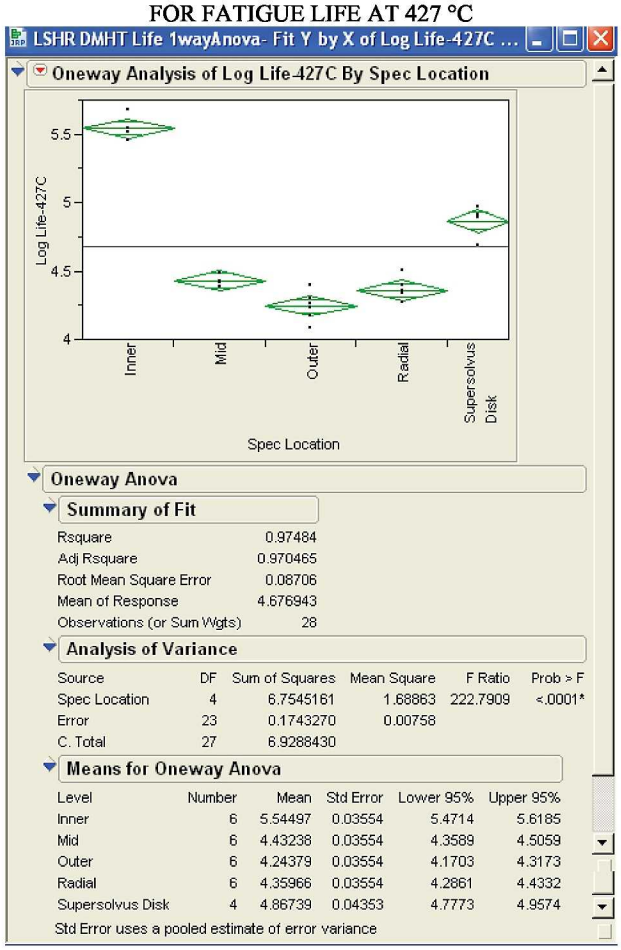

TABLE 1b.—COMPARISON OF MEAN
FATIGUE LIVES AT 427 °C

Comparisons for each pair using Student's t

t	Alpha
2.06866	0.05

Abs(Dif)-LSD

	Inner	Supersolvus Disk	Mid	Radial	Outer
Inner	-0.1040	0.5613	1.0086	1.0813	1.1972
Supersolvus Disk	0.5613	-0.1273	0.3188	0.3915	0.5073
Mid	1.0086	0.3188	-0.1040	-0.0313	0.0846
Radial	1.0813	0.3915	-0.0313	-0.1040	0.0119
Outer	1.1972	0.5073	0.0846	0.0119	-0.1040

Positive values show pairs of means that are significantly different.

Level		Mean
Inner	A	5.5449727
Supersolvus Disk	B	4.8673900
Mid	C	4.4323804
Radial	C	4.3596637
Outer	D	4.2437916

Levels not connected by same letter are significantly different.

Level	- Level	Difference	Lower CL	Upper CL	p-Value
Inner	Outer	1.301181	1.19720	1.405160	<.0001*
Inner	Radial	1.185309	1.08133	1.289288	<.0001*
Inner	Mid	1.112592	1.00861	1.216571	<.0001*
Inner	Supersolvus Disk	0.677583	0.56133	0.793835	<.0001*
Supersolvus Disk	Outer	0.623598	0.50735	0.739851	<.0001*
Supersolvus Disk	Radial	0.507726	0.39147	0.623978	<.0001*
Supersolvus Disk	Mid	0.435010	0.31876	0.551262	<.0001*
Mid	Outer	0.188589	0.08461	0.292568	0.0010*
Radial	Outer	0.115872	0.01189	0.219851	0.0305*
Mid	Radial	0.072717	-0.03126	0.176696	0.1615

TABLE 1c.—ONE-WAY ANALYSIS OF VARIANCE FOR FATIGUE LIFE AT 704 °C

LSHR DMHT Life 1wayAnova- Fit Y by X of Log Facet Area-427C ...

Oneway Analysis of Log Facet Area-427C By Spec Location

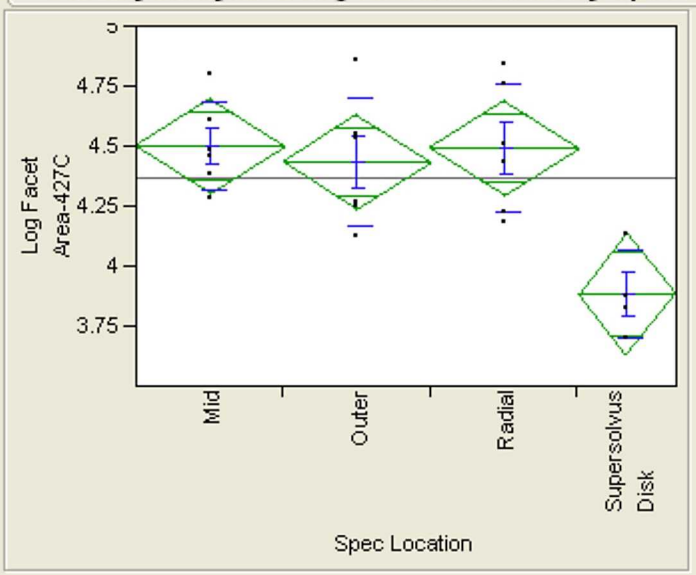

Missing Rows 6

Oneway Anova

Summary of Fit

Rsquare	0.541109
Adj Rsquare	0.464627
Root Mean Square Error	0.234153
Mean of Response	4.3675
Observations (or Sum Wgts)	22

Analysis of Variance

Source	DF	Sum of Squares	Mean Square	F Ratio	Prob > F
Spec Location	3	1.1637109	0.387904	7.0750	0.0024*
Error	18	0.9868940	0.054827		
C. Total	21	2.1506049			

Means for Oneway Anova

Level	Number	Mean	Std Error	Lower 95%	Upper 95%
Mid	6	4.50255	0.09559	4.3017	4.7034
Outer	6	4.43080	0.09559	4.2300	4.6316
Radial	6	4.49188	0.09559	4.2911	4.6927
Supersolvus Disk	4	3.88340	0.11708	3.6374	4.1294

Std Error uses a pooled estimate of error variance

TABLE 1d.—COMPARISON OF MEAN
FATIGUE LIVES AT 704 °C

Means Comparisons

Comparisons for each pair using Student's t

t	Alpha
2.07387	0.05

Abs(Dif)-LSD

	Inner	Supersolvus Disk	Mid	Radial	Outer
Inner	-0.1915	0.5178	1.3566	1.4602	1.5434
Supersolvus Disk	0.5178	-0.2709	0.5611	0.6648	0.7480
Mid	1.3566	0.5611	-0.1915	-0.0879	-0.0047
Radial	1.4602	0.6648	-0.0879	-0.1915	-0.1083
Outer	1.5434	0.7480	-0.0047	-0.1083	-0.1915

Positive values show pairs of means that are significantly different.

Level		Mean
Inner	A	6.1734011
Supersolvus Disk	B	5.4210308
Mid	C	4.6252868
Radial	C	4.5216386
Outer	C	4.4384083

Levels not connected by same letter are significantly different.

Level	- Level	Difference	Lower CL	Upper CL	p-Value
Inner	Outer	1.734993	1.54345	1.926539	<.0001*
Inner	Radial	1.651763	1.46022	1.843308	<.0001*
Inner	Mid	1.548114	1.35657	1.739660	<.0001*
Supersolvus Disk	Outer	0.982623	0.74803	1.217217	<.0001*
Supersolvus Disk	Radial	0.899392	0.66480	1.133987	<.0001*
Supersolvus Disk	Mid	0.795744	0.56115	1.030339	<.0001*
Inner	Supersolvus Disk	0.752370	0.51778	0.986965	<.0001*
Mid	Outer	0.186879	-0.00467	0.378424	0.0554
Mid	Radial	0.103648	-0.08790	0.295194	0.2739
Radial	Outer	0.083230	-0.10832	0.274776	0.3773

TABLE 2a.—ONE-WAY ANALYSIS OF VARIANCE FOR FACET AREA AT 427 °C

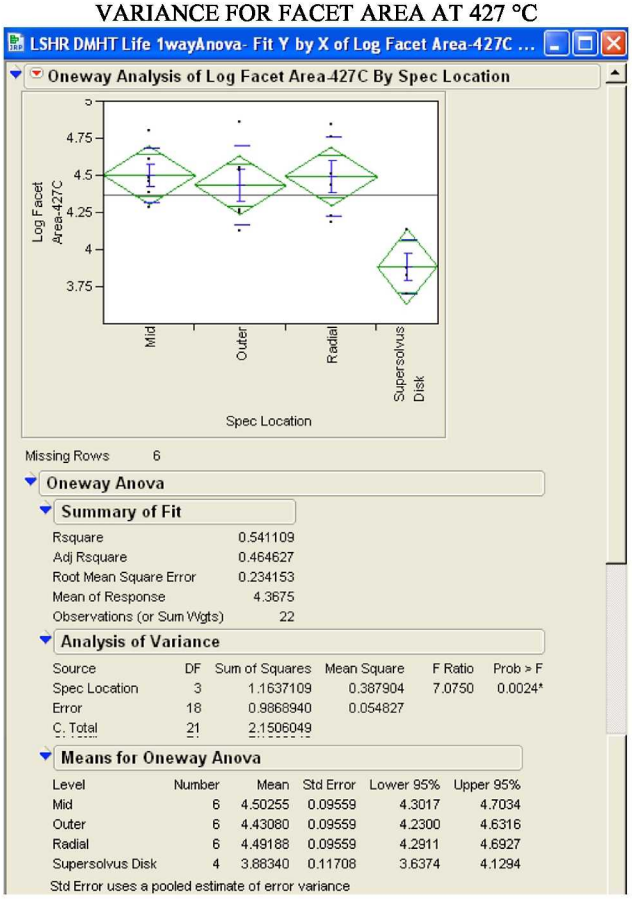

TABLE 2b.—COMPARISON OF MEAN FACET AREAS AT 427 °C

Means Comparisons

Comparisons for each pair using Student's t

t	Alpha
2.10092	0.05

Abs(Dif)-LSD

	Mid	Radial	Outer	Supersolvus Disk
Mid	-0.28402	-0.27335	-0.21227	0.30161
Radial	-0.27335	-0.28402	-0.22294	0.29094
Outer	-0.21227	-0.22294	-0.28402	0.22986
Supersolvus Disk	0.30161	0.29094	0.22986	-0.34785

Positive values show pairs of means that are significantly different.

Level		Mean
Mid	A	4.5025500
Radial	A	4.4918833
Outer	A	4.4308000
Supersolvus Disk	B	3.8834000

Levels not connected by same letter are significantly different.

Level	- Level	Difference	Lower CL	Upper CL	p-Value
Mid	Supersolvus Disk	0.6191500	0.301606	0.9366936	0.0007*
Radial	Supersolvus Disk	0.6084833	0.290940	0.9260269	0.0008*
Outer	Supersolvus Disk	0.5474000	0.229856	0.8649436	0.0020*
Mid	Outer	0.0717500	-0.212270	0.3557696	0.6021
Radial	Outer	0.0610833	-0.222936	0.3451029	0.6568
Mid	Radial	0.0106667	-0.273353	0.2946863	0.9380

TABLE 2c.—ONE-WAY ANALYSIS OF VARIANCE
FOR FACET AREA AT 704 °C

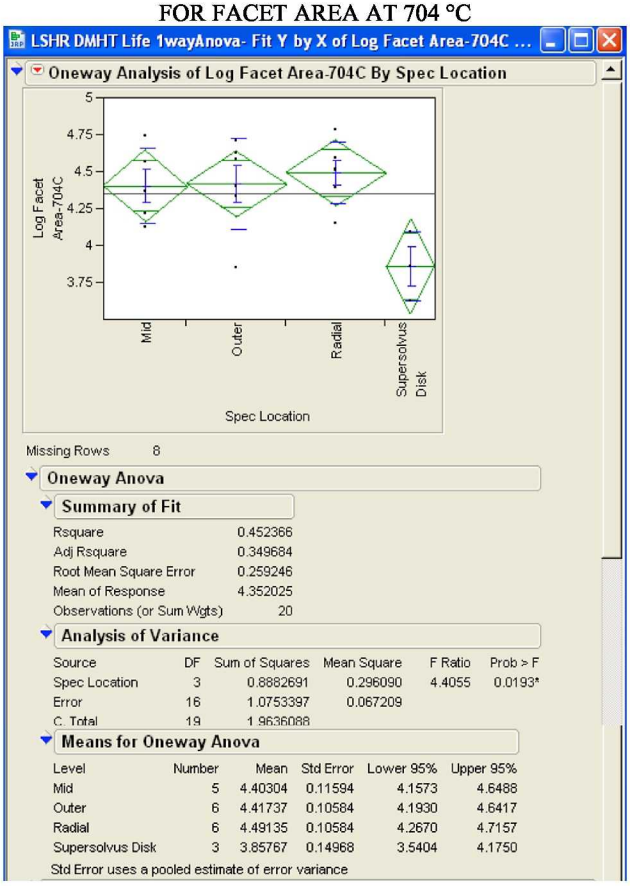

TABLE 2d.—COMPARISON OF MEAN FACET AREAS AT 704 °C

Means Comparisons

Comparisons for each pair using Student's t

t	Alpha
2.11991	0.05

Abs(Dif)-LSD

	Radial	Outer	Mid	Supersolvus Disk
Radial	-0.31730	-0.24332	-0.24448	0.24507
Outer	-0.24332	-0.31730	-0.31846	0.17109
Mid	-0.24448	-0.31846	-0.34758	0.14402
Supersolvus Disk	0.24507	0.17109	0.14402	-0.44873

Positive values show pairs of means that are significantly different.

Level		Mean
Radial	A	4.4913500
Outer	A	4.4173667
Mid	A	4.4030400
Supersolvus Disk	B	3.8576667

Levels not connected by same letter are significantly different.

Level	- Level	Difference	Lower CL	Upper CL	p-Value
Radial	Supersolvus Disk	0.6336833	0.245073	1.022294	0.0032*
Outer	Supersolvus Disk	0.5597000	0.171090	0.948310	0.0076*
Mid	Supersolvus Disk	0.5453733	0.144018	0.946728	0.0109*
Radial	Mid	0.0883100	-0.244476	0.421096	0.5815
Radial	Outer	0.0739833	-0.243316	0.391282	0.6278
Outer	Mid	0.0143267	-0.318459	0.347113	0.9284

REPORT DOCUMENTATION PAGE		Form Approved OMB No. 0704-0188

The public reporting burden for this collection of information is estimated to average 1 hour per response, including the time for reviewing instructions, searching existing data sources, gathering and maintaining the data needed, and completing and reviewing the collection of information. Send comments regarding this burden estimate or any other aspect of this collection of information, including suggestions for reducing this burden, to Department of Defense, Washington Headquarters Services, Directorate for Information Operations and Reports (0704-0188), 1215 Jefferson Davis Highway, Suite 1204, Arlington, VA 22202-4302. Respondents should be aware that notwithstanding any other provision of law, no person shall be subject to any penalty for failing to comply with a collection of information if it does not display a currently valid OMB control number.
PLEASE DO NOT RETURN YOUR FORM TO THE ABOVE ADDRESS.

1. REPORT DATE (DD-MM-YYYY)	2. REPORT TYPE	3. DATES COVERED (From - To)
01-04-2010	Technical Memorandum	

4. TITLE AND SUBTITLE
Fatigue Resistance of the Grain Size Transition Zone in a Dual Microstructure Superalloy Disk

5a. CONTRACT NUMBER

5b. GRANT NUMBER

5c. PROGRAM ELEMENT NUMBER

6. AUTHOR(S)
Gabb, T., P.; Kantzos, P., T.; Telesman, J.; Gayda, J.; Sudbrack, C., K.; Palsa, B., S.

5d. PROJECT NUMBER

5e. TASK NUMBER

5f. WORK UNIT NUMBER
WBS 698259.02.07.03.04.02

7. PERFORMING ORGANIZATION NAME(S) AND ADDRESS(ES)
National Aeronautics and Space Administration
John H. Glenn Research Center at Lewis Field
Cleveland, Ohio 44135-3191

8. PERFORMING ORGANIZATION REPORT NUMBER
E-17305

9. SPONSORING/MONITORING AGENCY NAME(S) AND ADDRESS(ES)
National Aeronautics and Space Administration
Washington, DC 20546-0001

10. SPONSORING/MONITOR'S ACRONYM(S)
NASA

11. SPONSORING/MONITORING REPORT NUMBER
NASA/TM-2010-216369

12. DISTRIBUTION/AVAILABILITY STATEMENT
Unclassified-Unlimited
Subject Category: 07
Available electronically at http://gltrs.grc.nasa.gov
This publication is available from the NASA Center for AeroSpace Information, 443-757-5802

13. SUPPLEMENTARY NOTES
Submitted to International Journal of Fatigue

14. ABSTRACT
Mechanical property requirements vary with location in nickel-based superalloy disks. To maximize the associated mechanical properties, heat treatment methods have been developed for producing tailored microstructures. In this study, a specialized heat treatment method was applied to produce varying grain microstructures from the bore to the rim portions of a powder metallurgy processed nickel-based superalloy disk. The bore of the contoured disk consisted of fine grains to maximize strength and fatigue resistance at lower temperatures. The rim microstructure of the disk consisted of coarse grains for maximum resistance to creep and dwell crack growth at high temperatures up to 704 °C. However, the fatigue resistance of the grain size transition zone was unclear, and needed to be evaluated. This zone was located as a band in the disk web between the bore and rim. Specimens were extracted parallel and transverse to the transition zone, and multiple fatigue tests were performed at 427 and 704 °C. Mean fatigue lives were lower at 427 °C than for 704 °C. Specimen failures often initiated at relatively large grains, which failed on crystallographic facets. Grain size distributions were characterized in the specimens, and related to the grains initiating failures as well as location within the transition zone. Fatigue life decreased with increasing maximum grain size. Correspondingly, mean fatigue resistance of the transition zone was slightly higher than that of the rim, but lower than that of the bore. The scatter in limited tests of replicates was comparable for all transition zone locations examined.

15. SUBJECT TERMS
Gas turbine engines; Rotating disks; Heat resistant alloys; Fatigue

16. SECURITY CLASSIFICATION OF:			17. LIMITATION OF ABSTRACT	18. NUMBER OF PAGES	19a. NAME OF RESPONSIBLE PERSON
a. REPORT	b. ABSTRACT	c. THIS PAGE			STI Help Desk (email:help@sti.nasa.gov)
U	U	U	UU	30	19b. TELEPHONE NUMBER (include area code) 443-757-5802